Vol. 01 (2025) 68-78, DOI: 10.61552/EC.2025.005

Energy Catalyst

www.jme.aspur.rs

Experimental Investigation of a Vertical Flow Moving Bed Thermochemical Heat Storage

Devrim Aydin[a,b,*], Hasila Jarimi[a], Behiye Yuksel[c], Zafer Utlu[c], Saffa Riffat[a]

[a]*Department of Architecture and Built Environment, University of Nottingham, University Park, Nottingham, NG7 2RD, UK,*
[b]*Department of Mechanical Engineering, Eastern Mediterranean University, G. Magosa, TRNC Mersin 10, Turkiye 2RD, UK,*
[c]*Faculty of Engineering and Natural Sciences, Istanbul Atlas University, 34408, Istanbul, Türkiye.*

Keywords:

Thermochemical Heat Storage, Movıng Bed, Solar Energy, Sorbent, Experimental

* Corresponding author:

Devrim Aydin
E-mail:
devrim.aydin1@nottingham.ac.uk

Received: 27 January 2025
Revised: 15 March 2025
Accepted: 18 May 2025

A B S T R A C T

Thermochemical heat storage has the potential to enhance solar share in building heating systems. However, the limitation of heat and mass transfer in fixed-bed thermochemical heat storage is one of the main barriers in implementation of this technology in real life applications. In order to address this problem, a new solar driven vertical flow moving bed thermochemical heat storage system has been developed and tested in present study. According to the testing results, discharging temperature lift up to 30 °C was achieved. Meanwhile, the total moisture uptake of the sorbent was varied between 310-435 g. On the other hand, solar radiation was in the range of 0.74-0.81 kW/m2 during the charging process. Air temperature between 66-72 °C was obtained during different tests. Based on the solar heat gain of air and the rate of heat transfer to the sorbent inside the reactor, charging efficiency of the system was found between 0.37-0.51. Study results revealed that moving bed THS design is promising for enhancing and stabilizing the heat storage performance. However system optimization and process control are key aspects for further development of moving bed reactors.

1. INTRODUCTION

Solar energy is one of the key sources to be utilized for reducing the fossil fuel consumption in buildings. Particularly for building space heating, solar energy represents an excellent potential. However due to the mismatch between the solar availability and the building heating demand, it is challenging to make use of solar energy in the built environment [1]. Utilizing thermal energy storage (TES) in solar systems is the key solution to this problem; however, the current TES systems provide low energy storage density resulting with bulky system size, which also leads to high investment costs and large space requirement. More

importantly current sensible and latent heat storage methods can only store the heat over a short period (i.e. daily) which is not sufficient for the development of a reliable solar sourced heating system [2]. As an emerging technology, thermochemical heat storage (THS) represents important advantages; those can overcome the abovementioned problems of sensible and latent heat storage methods. As THS stores the heat as a chemical potential, the heat loss during the storage period is negligible, enabling long term heat storage (i.e. seasonal) [3]. In addition, THS presents higher heat storage density in comparison with other heat storage methods, which is advantageous for reducing the space requirement in real life applications [4].

Despite the numerous efforts, THS development is still not at the desired level. Particularly the research on effective reactor configurations is ongoing. Several different designs have been studied previously with the aim of increasing the heat and mass transfer performances. A fixed-bed THS unit is experimentally investigated by Salama et al. [5]. Composite sorbent consisting of $MgSO_4$, expanded graphite and ammonium persulfate is synthesized and used in the study. Based on the testing results, energy density and sorption energy efficiency varied between 11.7-335.8 MJ/m^3 and 28.3-79.1%, respectively. In another study, Beaupere et al. [6] developed and tested a novel THS reactor using ettringite as the sorbent. With the use of 0.05 m^3 material, energy storage density of 50 MJ/m^3 is obtained during the discharging process. Zeng et al. [7] evaluated various building integration strategies of open-THS reactors. Authors simulate the thermal performance of different THS designs across a range of building types and climates. Based on the study results, authors highlighted that the system configuration, supply air relative humidity and the climate conditions have key importance on the THS performance in practical applications. Farcot et al. [8] developed a 1 kW moving bed THS reactor using $SrBr_2$ as the sorption material. Based on the experimental results, reactor temperature reached to 41°C while specific heating power varied between 1.7–4.6 kW/m^3. In a recent study, Zhang et al. [9] compared tubular and plate-type modular reactors for THS applications. A 4-5 times lower pressure drop is obtained with tubular type reactors with a 7% higher equivalent thermal efficiency in comparison with plate type reactor. In order to provide a solution to unstable discharging thermal output in single bed THS reactors, Zhang et al. [10] developed a dual material reactor. In the developed reactor, AA-15% LiCl composite and $SrBr_2{\cdot}H_2O$ were used as two different bed materials. According to the study results, the discharging/charging energy efficiency was increased by 0.4–1.7 times compared with single-material reactor. In another experimental study, Al Ghosini and Aydin [11] evaluate the performance of pumice and vermiculite based salt-in-matrix composite sorbents in a fixed-bed reactor. Based on the testing results, highest energetic and exergetic efficiencies were obtained as 74% and 17.5%, respectively. Karim Nejhad et al. [12] investigated a solar-integrated reactor for low grade THS applications. During the discharging experiments, the inlet air had a temperature and humidity range of 21–24°C and 80-90%. Under these conditions, the system achieved an average energy output of 2.1 kWh, with an energy storage density averaging 156 kWh/m^3. The charging process utilized an average of 5.6 kWh of solar energy and 1.8 kWh of desorption energy. Based on the charging tests, the moisture desorption rate and system cyclic efficiency were found as 6.5 g/min and 38%. Chen et al. [13] evaluated the impact of different porous host materials on the THS performance. Based on the results, the mesoporous SG-$CaCl_2$ composite showed high reaction rates and hydration capacity, delivering a sustained temperature rise of 16.01 °C at 50% RH, though with a notable pressure drop (101.06 Pa) across a 5 cm bed at 0.2 m/s airflow. In contrast, EP-$CaCl_2$ offered smoother heat release, lower resistance (6.88 Pa), and a solid volumetric energy density of 0.65 GJ/m^3. In another study, Wang et al. [14] developed a composite of $MgCl_2$ and natural coral aggregate ($MgCl_2$-CA) for THS using vacuum impregnation. Compared to zeolite 13X, the 35% $MgCl_2$-CA exhibited lower heat storage density and pressure loss, but delivered significantly higher useful heat output under equal pump power. Despite challenges in maintaining salt content, the material showed strong potential for cost-effective energy storage applications. In a simulation study on THS system, Berut et al. [15] examined how the selection of a sorption isotherm model affects the results. To achieve this, three models are analyzed: the Langmuir, Dubinin-Astakhov (DA), and modified Brunauer-Emmett-Teller (BET)

isotherms. A one-dimensional model of an open fixed-bed reactor, which operates based on the hydration and dehydration processes of zeolite 13X, is developed. Among the models considered, the BET isotherm proved to be the most suitable for describing water adsorption on zeolite 13X, as it accounts for multilayer adsorption phenomena. In another modelling work, Kiskamp et al. [16] analysed and validated kinetics of K_2CO_3. Utilizing the established kinetic model, a numerical simulation of a packed particle bed was constructed using a coupled CFD-DEM (Computational Fluid Dynamics–Discrete Element Method) framework. The simulation results showed strong agreement with experimental data from a particle bed system. The developed modular setup demonstrated the ability to provide 10 kW of thermal power at 45 °C for a continuous duration of 19.5 hours.

Based on the previous literature, fixed-bed THS reactors were heavily researched. Although the fixed-bed reactors represent simplicity in manufacturing and operation, they represent significant drawbacks. With the increase in the bed thickness, the pressure drop dramatically increases which results in the drop of system performance. In addition, with the reduction of permeability of sorbent material due to the hydration in discharging, air cannot uniformly diffuse through the sorption bed. In order to address these problems of fixed-bed THS reactors, a moving-bed continuous THS reactor is developed and experimentally investigated in this study. The THS reactor is also integrated with a flat-plate solar collector system for evaluating the charging performance of the developed unit.

2. MATERIALS AND METHODS

2.1 System Description

Within the study, solar driven continuous thermochemical heat storage (CTHS) system was designed and developed, consisting of a storage chamber at the top, a material flow chamber beneath it, and a reaction chamber at the bottom. This configuration allows the material to move from top to bottom under the influence of gravity. The schematic representation of the system's operating principle is presented in Figure 1.

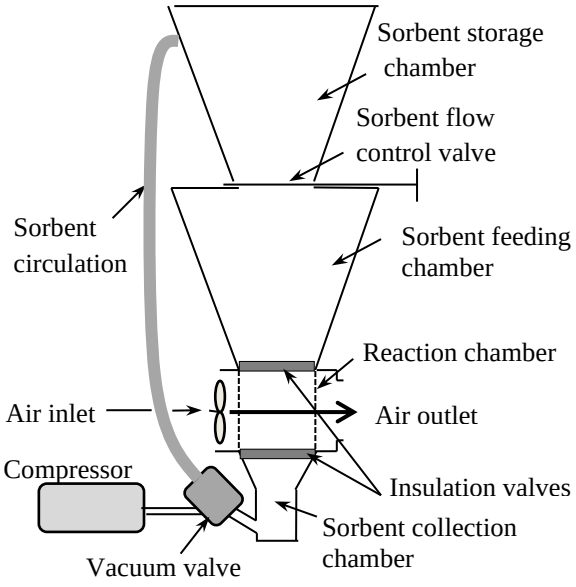

Fig. 1. Schematic illustration of the developed horizontal flow CTHS system.

The system is constructed from galvanized metal, with the inner surfaces of the chambers coated with varnish to prevent corrosion and reduce friction. A 150 mm diameter metal duct fan was utilized to facilitate airflow. To prevent degradation of the material tested within the system, the sorption material was fed back into the storage tank via a vacuum system at the end of the discharge/charge process. In this vacuum system, suction was achieved by supplying compressed air to a vacuum valve integrated into the feed pipe, creating a vacuum in the direction of the pipe flow. This method allowed the material to be transferred from the lower section back to the storage tank. Since this material transport occurs only at the end of the process, the compressor's operating time is very short, and the energy consumption of the compressor has a negligible impact on process performance.

The vertically-oriented continuous-flow CTHS system, detailed above, was integrated with solar collectors. In the system, the composite sorbent, consisting of $CaCl_2$ impregnated into pumice stone, was tested. The schematic representation of the developed process is shown in Figure 2. A solar flat-plate water heater was employed in the system to charge the composite sorbent. Additionally, a water-to-air heat exchanger was used to transfer heat from the water to the charging air.

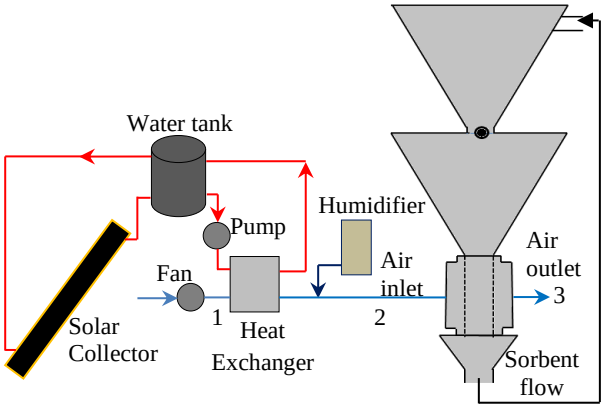

Fig. 2. Schematic illustration of the experimental solar driven THS system.

The solar collector has dimensions of 940 mm in width and 1940 mm in length, providing a total surface area of 1.82 m^2. To minimize heat losses from the rear of the collector, the backside of the collector is insulated with 50 mm thick glass wool. The experiments were conducted in July, during which both discharge and charging process tests were performed. In total, 9 discharge tests and 6 charging tests were carried out in the experimental study.

During the experiments, at the beginning of each cycle, the valve between the sorbent feeding chamber and the reaction chamber (Fig. 1) was opened allowing the reaction chamber to be filled with the sorbent due to the gravity driven flow. Following that, the valve is closed and discharging process was performed. Upon completion of the discharging process, the valve below the reaction chamber was opened and the material is transported to the sorbent storage chamber with the vacuum system. Upon discharging of all sorbent material, the hydrated sorbent accumulated inside the sorbent storage chamber was first transferred to the sorbent feeding chamber by opening the sorbent flow control valve (Fig. 1) and charged with the similar procedure of the discharging process.

A Sensirion data logger equipped with an SHTC3 sensor was utilized during the experiments to measure and record the temperature and relative humidity of the inlet, outlet, and ambient air. The temperature measurement range of the data logger was 0 to 140 °C with an accuracy of ±0.2 °C, while the relative humidity measurement range was 0 to 100% with an accuracy of ±2.0%. The air velocity at the system's outlet was determined using a weather anemometer (Xplorer GLX), which had a standard measurement range of 0 to 7 m/s and an accuracy of ±0.1 m/s. Additionally, the solar radiation was measured with a pyranometer which had a measurement range and accuracy of 0-2800 W/m2 and ±3.0 W/m2, respectively. For the thermodynamic analysis of the system, formulas presented in Section 2.2 were used to calculate discharging heat gain, charging heat transfer, and charging efficiencies.

2.2 Composite Sorbent Material Synthesis

In the study, natural porous pumice stone impregnated with $CaCl_2$ was used as a THS material. Pumice-$CaCl_2$ composite sorbent is promising material for THS due to its low cost, availability, and effective energy storage performance. Pumice serves as a porous host matrix with high porosity and moderate surface area, providing structural support and facilitating mass transfer. Its thermal stability and chemical inertness make it suitable for repeated hydration-dehydration cycles. Calcium chloride ($CaCl_2$), a highly hygroscopic salt, acts as the active sorbent component. It can undergo multiple reversible hydration reactions, enabling low/medium temperature heat storage. Impregnating pumice with $CaCl_2$ enhances thermal stability and helps contain the salt, reducing issues like deliquescence and agglomeration.

The production of the pumice-CaCl2 composite sorbent material began with the removal of the natural moisture contained inside the pumice stone. For this purpose, pumice was dried in an oven at 150°C for 24 hours. After the residual moisture was removed, the pumice was impregnated with a $CaCl_2$ solution prepared at a concentration of 75 g/100 mL. Following this, the moisture inside the salt-impregnated pumice was evaporated and removed by drying it at 150 °C for 12 hours. After these steps, the $CaCl_2$-impregnated natural pumice stones were stored in hermetically sealed chambers until the experimental period.

2.3 Governing equations

The heat output rate ($\dot{Q}_{out}$) in discharging and heat input rate in charging ($\dot{Q}_{in}$) are determined via Eqs. (1) and (2), respectively;

$$\dot{Q}_{out} = \dot{m}_d C_p (T_3 - T_2) \quad (1)$$

$$\dot{Q}_{in} = \dot{m}_c C_p (T_2 - T_3) \quad (2)$$

Where, T_2 and T_3 are reactor inlet and outlet temperatures, $\dot{m}_d$ and $\dot{m}_c$ are discharging and charging air mass flow rates.

The solar heat gain of process air across the heat exchanger during the charging process can be obtained with Eq. (3);

$$\dot{Q}_{sol} = \dot{m}_c C_p (T_2 - T_1) \quad (3)$$

The thermal efficiency of THS charging process is expressed by Eq. (5);

$$\eta_c = \frac{\dot{Q}_{in}}{\dot{Q}_{sol}} \quad (4)$$

The mass change of the sorbent due to the moisture adsorption and desorption in discharging and charging processes can be obtained as follows;

$$\Delta m_c = m_{d,f} - m_{c,f} \quad (5)$$

$$\Delta m_d = m_{d,f} - m_i \quad (6)$$

Where $m_{d,f}$ is the final mass of sorbent at the end of the discharging process, $m_{c,f}$ is the final mass of sorbent at the end of the charging process, and m_i is the initial dry mass of the sorbent.

The hygro-cyclic efficiency (η_{hyg}) of sorbent then can be determined via Eq. (7);

$$\eta_{hyg} = \frac{(m_{d,f} - m_{c,f})_{ave}}{(m_{d,f} - m_{i)_{ave}}} \quad (7)$$

The uncertainties of the experimental results were determined using Gauss's propagation law to calculate the percentage errors. According to this method, the uncertainty of individual independent variables (w_R) is represented by the variables w_1, w_2, w_3, …, w_n [17];

$$w_R = \left[\left(\frac{\partial R}{\partial x_1} w_1\right)^2 + \left(\frac{\partial R}{\partial x_2} w_2\right)^2 + \left(\frac{\partial R}{\partial x_3} w_3\right)^2 + \cdots + \left(\frac{\partial R}{\partial x_n} w_n\right)^2\right]^{1/2} \quad (8)$$

The total uncertainty of η_c, could be obtained by solving Eq. 8 based on the main function partial derivatives and the uncertainty of independent variables (T_1, $T_2, T_3, \dot{m}_c$). Thus, the total uncertainty of η_I could be determined via Eq. 9;

$$w_{\eta_c} = \left[\left(\frac{\partial \eta_c}{\partial T_1} w_{T_1}\right)^2 + \left(\frac{\partial \eta_c}{\partial T_2} w_{T_2}\right)^2 + \left(\frac{\partial \eta_c}{\partial T_3} w_{T_3}\right)^2 + \left(\frac{\partial \eta_c}{\partial m_c} w_{\dot{m}_c}\right)^2\right]^{1/2} \quad (9)$$

Based on the Eq. (9) the maximum uncertainty of η_c is obtained as 4.36%.

3. RESULTS AND DISCUSSION

3.1 Discharging Process Analyses

The discharge process was conducted during the morning hours of 08:00–10:00 when ambient air temperatures were relatively moderate. During the experiments, the inlet air temperatures ranged between 24–29 °C, while discharge temperatures, influenced by moisture absorption, were recorded within the range of 30–55 °C. A total of nine discharge cycles were performed throughout the experiments.

As shown in Figure 3, discharge temperatures close to 60 °C were achieved during the first two cycles, which can be attributed to the fully dried state of the material. However, in subsequent cycles, peak temperatures were typically observed in the range of 40–50 °C. This behaviour is attributed to the undesired ingress of moisture inside the storage tank and partial hydration of sorbent before entering the reaction chamber. Despite this, the material demonstrated stable performance over the remaining seven discharge cycles (following the second cycle), which is considered a positive outcome. To achieve complete charging of the material, higher charging

temperatures are necessary. This can be accomplished by increasing the collector surface area or with the use of an auxiliary electric heater powered by photovoltaic panels.

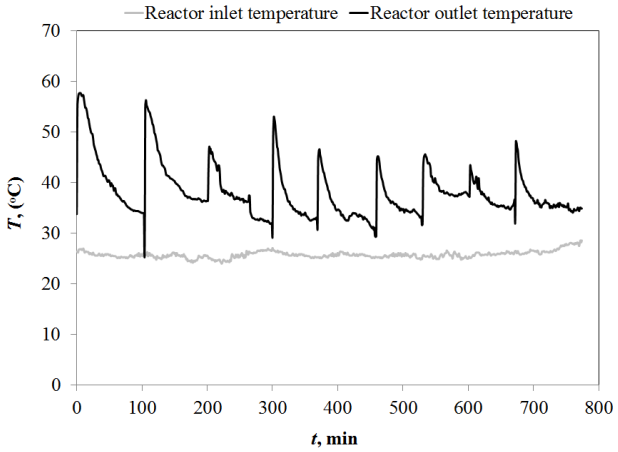

Fig. 3. Cyclic temperature variations during the discharging process.

The heat outputs for the nine repeated discharge cycles are presented in Figure 4. Since heat output is a function of temperature, the average heat output profiles exhibit a trend consistent with the temperature profiles shown in Figure 4. In the first two cycles, an average heat output of approximately 0.3 kW was achieved, while subsequent cycles produced outputs exceeding 0.2 kW. Notably, a heat output of 0.25 kW was observed during the 7th cycle. This anomaly can likely be attributed to higher ambient humidity levels compared to other cycles, resulting in increased moisture absorption. The generally low heat outputs observed are due to the small-scale experimental design of the vertical-flow system's test bed, with a limited volume of ~0.001 m^3. Consequently, the airflow rate used in the experiments was also low, at 0.018 kg/s.

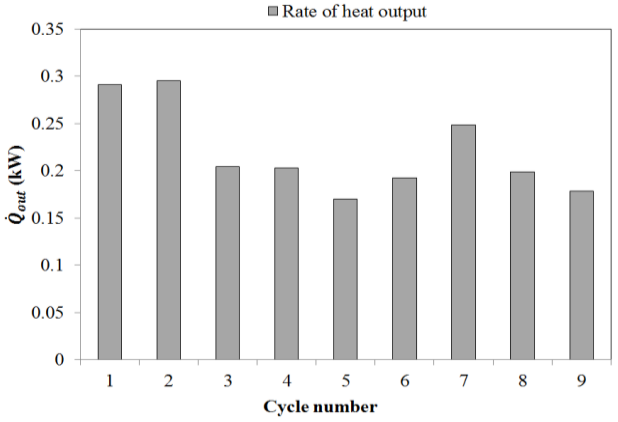

Fig. 4. Average discharging heat output over the repeating cycles.

Figure 5 illustrates the amounts of moisture absorbed during the discharge processes and the corresponding mass changes in the sorption material. Although a similar volume of sorbent was used at the beginning of each discharge experiment, the dry sorbent mass was expected to remain approximately constant. However, the dry mass increased from 702 g in the initial cycle to 902 g by the 9th cycle, indicating unintended moisture ingress into the sorbent feeding chamber over the course of the experiments. This explains the decline in temperature and heat output values over successive cycles, as shown in Figures 3 and 4.

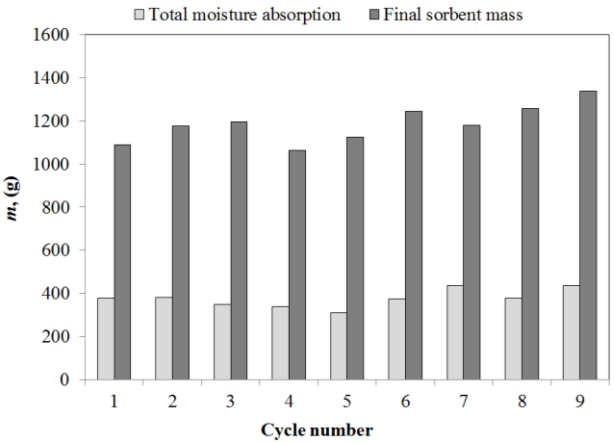

Fig. 5. Total moisture absorption and sorbent mass variations over the repeating discharging cycles.

When examining the moisture absorption amounts during the cycles presented in Figure 5, fluctuations were observed without a distinct increasing or decreasing trend. Although the differences in moisture absorption amounts were not significant, the initial moisture content of the materials increased over successive cycles, explaining the observed performance drop during consecutive discharge processes.

3.2 Charging Process Analyses

The temperature variations at different points during the charging processes are presented in Figure 6. Measurements included ambient temperature, collector outlet water temperature, heat exchanger outlet/reactor inlet temperature, and reactor outlet temperature. During the experiments, ambient temperatures ranged between 30–40 °C, while collector outlet water temperatures were measured in the range of 80–90 °C.

Consequently, ambient air passed through the water-to-air heat exchanger unit and was heated to approximately 70 °C using the collector outlet water. Fluctuations in water temperature at the heat exchanger outlet were attributed to variations in ambient temperature. Hot and dry air at 70 °C was supplied to the sorbent in the reactor, where the reactor air outlet temperature dropped to near 50 °C and gradually increased during the charging process. This temperature rise was primarily due to the high initial moisture content of the sorbent, which decreased as desorption progressed, reducing the rate of water removal from the sorbent.

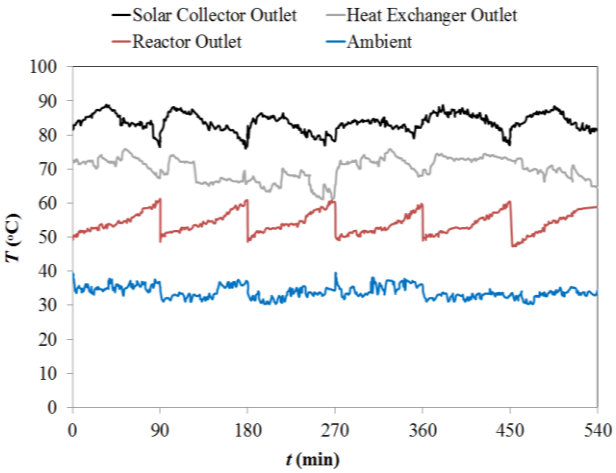

Fig. 6. Temperature variations at different measurement points during the charging process.

The reactor outlet temperature profiles during repeated experiments showed similar trends, increasing from 50 °C to approximately 60 °C as the process advanced.

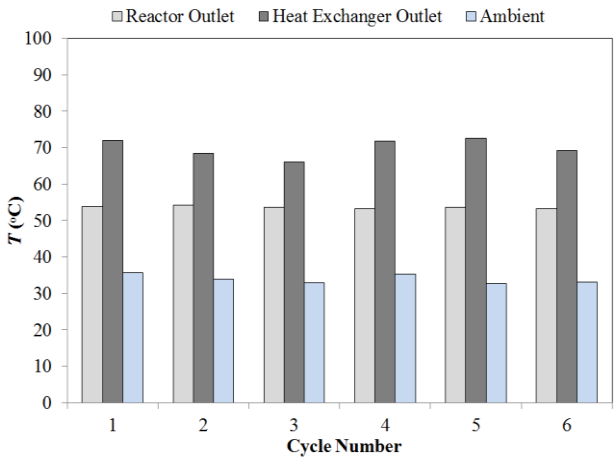

Fig. 7. Cyclic average reactor outlet, heat exchanger outlet and ambient temperatures during the charging process.

Figure 7 shows the reactor inlet (heat exchanger outlet), reactor outlet, and average ambient temperatures over six repeated cycles. Across all cycles, the average reactor inlet temperatures remained consistent around 70 °C, while the average reactor outlet temperatures varied between 50–55 °C. Additionally, the ambient temperatures during the experiments ranged from 30–35 °C. The 15–20 °C temperature difference observed across the reactor bed is attributed to the energy consumption required for moisture desorption from the inlet air within the reactor. Solar radiation measurements recorded during the experiments are presented in Figure 8. The average solar radiation values ranged 700–800 W/m^2, showing stability within this range throughout the experimental period.

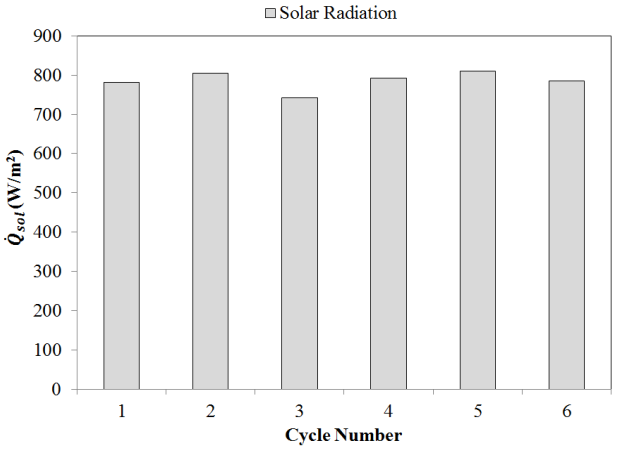

Fig. 8. Average solar radiation during different charging cycles.

Figure 9 presents the average values of solar energy gain in the heat exchanger and the heat transferred to the reactor during six repeated charging processes. The solar energy gain in the heat exchanger refers to the amount of heat transferred from the water heated in the solar collector to the charging air. The heat transferred to the reactor represents the energy change between the reactor inlet and outlet air. According to the data, the solar energy gain in the heat exchanger ranged between 0.6–0.7 kW across the cycles, while the heat transferred to the reactor varied between 0.2–0.35 kW. A portion of the energy carried by the air passing through the sorption bed was utilized for moisture desorption, with the remaining energy being released into the environment along with the humid air. Utilizing the waste heat from the desorption exhaust air for preheating the inlet air is identified as a parameter that could

enhance system efficiency. Future studies could focus on this aspect to implement improvements in system performance.

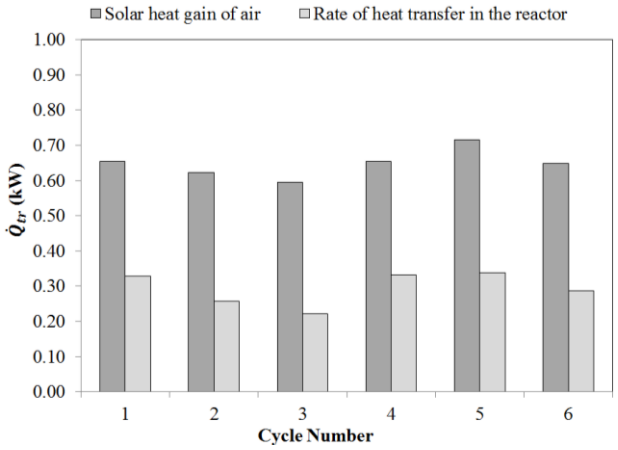

Fig. 9. Solar heat gains and heat transfer rates across the reactor during different charging cycles.

The calculated thermal efficiencies of the charging process, based on the solar energy gain and heat transferred to the reactor presented in Figure 9, are shown in Figure 10. The charging thermal efficiency was determined as the ratio of the heat transferred to the reactor to the solar energy gain, representing the proportion of solar energy utilized in the charging process.

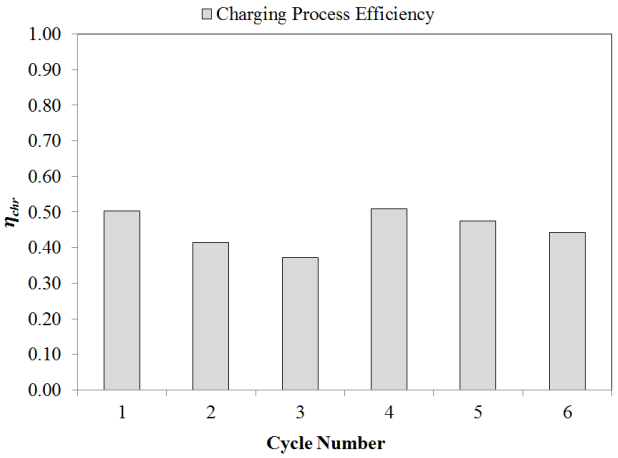

Fig. 10. Charging efficiency of different charging cycles.

The thermal efficiencies of the charging process ranged between 36% and 54%, with a ~18% difference observed between the highest and lowest values across the cycles. The lowest thermal efficiency (<40%) was recorded during the third cycle. This was attributed to a reduction in solar energy gain during that cycle, leading to decreased heat transfer to the reactor. As solar energy gain diminished, the temperature of the reactor inlet air dropped, resulting in a lower desorption of moisture from the sorbent. Since the amount of heat transferred to the reactor correlates with the amount of moisture desorbed, this decrease further reduced the thermal efficiency of the charging process.

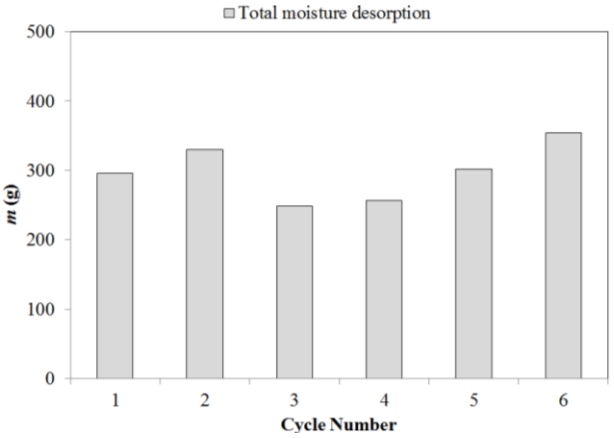

Fig 11. Total moisture desorption from the sorbent during different charging cycles.

Figure 11 illustrates the moisture desorption amounts during repeated charging processes. The moisture desorption is influenced by various parameters, including the amount of solar energy gained, the relative humidity of ambient air, and the water content inside the sorbent material. As shown in the figure, the moisture desorption amounts ranged between 250–350 g across the cycles. By comparison, the average moisture absorption values during the discharge process, presented in Figure 5, were calculated to be approximately 375 g per cycle. The average desorption amount, however, was determined to be 297 g. These results indicate that approximately 80% of the moisture absorbed during the discharge process could be desorbed during the charging process. This is also defined as the η_{hyg} of the THS process. The primary reason for this incomplete desorption is attributed to the inability to achieve the required charging temperatures (>80 °C).

The development of gravity-driven moving bed THS system investigated in this study presents several advantages compared to traditional fixed-bed configurations. Most notably, the dynamic movement of the THS material (sorbent) in a moving bed allows for enhanced heat/mass transfer, leading to improved thermal efficiency and more uniform reaction conditions.

Additionally, the moving bed concept enables better control over reaction front progression, potentially leading to more complete material utilization and easier thermal management. This makes the system particularly attractive for medium-to long-duration energy storage applications in solar thermal and waste heat recovery contexts. Despite its potential, the study highlights several limitations (given below) of the proposed moving bed design that must be addressed for practical deployment:

Use of Metallic Storage Chambers: The employment of metal-based reaction chambers introduces the risk of corrosion, especially under the high humidity or chemically aggressive conditions often found in salt hydrate based THS systems. This may impact system longevity and reliability.

Low Power Density: The small scale of the reaction unit utilized in the investigated prototype limits the system's power density. This makes it less suitable for applications requiring high thermal output, and scale-up strategies must be considered in future work.

Heat Loss: Due to the increased surface area and possible thermal bridging in the moving bed configuration, there may be significant heat losses to the environment, especially in poorly insulated segments. This reduces overall round-trip efficiency.

Air Infiltration at Separation Valves: The proposed moving bed design requires the use of separation or sealing valves to control the flow of sorbent between chambers. These valves can be prone to air leakage, leading to undesired ingress of vapour, thereby reduced process efficiency over the repeating cycles.

System and Flow Rate Optimization: The optimal size of the system and the flow rate of the sorbent needs to be determined. Improper flow rates can lead to insufficient reaction times or excessive pressure drops, adversely affecting system performance and control.

While the gravity-driven moving bed THS system demonstrates important improvements in system efficiency and performance stability over fixed bed alternatives, further work is necessary to address the practical limitations related to materials, scale-up, and thermal management. In addition system controls should be integrated for optimal operation. These findings provide a valuable foundation for future research in the field of THS.

4. CONCLUSION

In this study a vertical flow gravity driven moving bed THS system has been investigated. The results demonstrated that the proposed concept could enable intermittent operation of THS systems with effective process control. The material inside the sorption bed can be periodically replaced therefore large volume of THS material could be processed in a controlled way, depending on the demand. In current fixed bed THS systems, sorbent material storage and sorption/desorption processes occur in the same place which drives the need of advanced designs for enhancing the heat and mass transfer. Separating the storage and process sections as proposed in the current study, eliminates the need of using additional air flow channels modular designs or heat/mass transfer enhancement techniques. Furthermore, in a realistic THS system, when fixed bed is used, the bed thickness is a major concern due to the large pressure drop of air and limited/non-uniform penetration of air through the sorbent. In the proposed moving bed system, rather than increasing bed thickness to meet varying heat demand, the sorption bed replacement frequency can be adjusted, with optimal thickness selected during the design stage. The specific outcomes of the study can be summarized as follows;

The temperature lift during the discharging process in initial cycle reached to >25 ^{o}C in first two discharging cycles with average heat output values of ~0.3 kW. In the remaining cycles, heat output varied in the range of 0.17-0.24 kW.

The mass uptake ratio varied between 0.38 (5th cycle) and 0.58 (7th cycle), which was affected by the inlet air humidity levels as well as the initial state (i.e. moisture content) of the sorbent. The rest of the cycles provided relatively steadier mass uptake ratio varying between 0.41 and 0.52.

In charging period solar radiation was nearly steady and varied between 0.74-0.8 kW/m^2. The

solar energy transferred to the process air and the rate of heat transfer to the sorbent was found between 0.6-0.72 kW and 0.22-0.34 kW. Accordingly, charging efficiency was in the range of 0.37-0.51 over the repeating charging cycles.

The total moisture desorption in repeating charging cycles was fluctuated between 248-354 g, corresponding to cycle average moisture desorption of 298 g. For the discharging process, average cyclic value of moisture sorption was determined as 376 g. Accordingly, it was found that, on average, 79% of the moisture absorbed during each discharging cycle could be desorbed during the charging cycle using the developed solar heating system. This result highlights the promising potential of solar thermal energy storage with THS systems particularly in regions with high solar availability.

Acknowledgement

This work was supported by the Engineering and Physical Sciences Research Council [Horizon Europe Guarantee grant number: EP/Z002117/1] and the Scientific and Technological Research Council of Turkey [grant number: 119M073].

REFERENCES

[1] D. Gao, B. Zhao, T. H. Kwan, Y. Hao, and G. Pei, "The spatial and temporal mismatch phenomenon in solar space heating applications: status and solutions," Applied Energy, vol. 321, p. 119326, Sep. 2022, doi: 10.1016/j.apenergy.2022.119326.

[2] K. Moulakhnif et al., "Renewable approaches to building heat: exploring cutting-edge innovations in thermochemical energy storage for building heating," Energy and Buildings, vol. 318, p. 114421, Jun. 2024, doi: 10.1016/j.enbuild.2024.114421

[3] M. Karim Nejhad and D. Aydin, "Synthesize and hygro-thermal performance analysis of novel APC-CaCl2 composite sorbent for low-grade heat recovery, storage, and utilization," Energy Sources, Part A: Recovery, Utilization, and Environmental Effects, vol. 43, no. 23, pp. 3011–3031, Sep. 2019, doi: 10.1080/15567036.2019.1666187.

[4] A. B. Çolak, D. Aydin, A. Al-Ghosini, and A. S. Dalkilic, "Discharging performance prediction of experimentally tested sorption heat storage materials with machine learning method," Journal of Energy Storage, vol. 56, pp. 106159–106159, Nov. 2022, doi: 10.1016/j.est.2022.106159.

[5] M. A. Salama, S. A. Mohamed, M. Attalla, and A. N. Shmroukh, "Experimental investigation on a thermochemical seasonal sorption energy storage battery utilizing $MgSO_4$-H_2O," *Environmental Science and Pollution Research*, vol. 30, no. 43, pp. 98502–98525, Aug. 2023, doi: 10.1007/s11356-023-28875-1.

[6] N. Beaupere, A. Malley-Ernewein, T. Nahhas, S. Ginestet, G. Samson, and M. Cyr, "Experimental study of a thermochemical energy storage system operating at low temperature with ettringite-based materials," Solar Energy, vol. 282, p. 112927, Nov. 2024, doi: 10.1016/j.solener.2024.112927

[7] Y. Zeng et al., "Open-cycle thermochemical energy storage for building space heating: Practical system configurations and effective energy density," Applied Energy, vol. 376, pp. 124218–124218, Aug. 2024, doi: 10.1016/j.apenergy.2024.124218

[8] L. Farcot, N. Le Pierrès, and J.-F. Fourmigué, "Experimental investigation of a moving-bed heat storage thermochemical reactor with SrBr2/H2O couple," Journal of Energy Storage, vol. 26, p. 101009, Dec. 2019, doi: 10.1016/j.est.2019.101009.

[9] Y. Zhang, M. Hu, Z. Chen, Y. Su, and S. Riffat, "Exploring a novel tubular-type modular reactor for solar-driven thermochemical energy storage," Renewable Energy, vol. 221, p. 119767, Feb. 2024, doi: 10.1016/j.renene.2023.119767.

[10] Y. Zhang, T. Yan, and R. Wang, "A new strategy of dual-material reactors for stable thermal output of sorption thermal battery," *Energy*, vol. 293, pp. 130692–130692, Feb. 2024, doi: 10.1016/j.energy.2024.130692.

[11] Abdullah Al Ghosini and D. Aydin, "Comparative energy and exergy analyses of pumice and vermiculite-based salt-in-matrix composites for low-grade thermochemical heat storage applications," International Journal of Exergy, vol. 43, no. 3, pp. 273–286, Jan. 2024, doi: 10.1504/ijex.2024.137565.

[12] Majid Karim Nejhad, D. Aydin, and M. Rezaei, "Experimental investigation of a solar-charged sorption thermal battery," Proceedings of the Institution of Mechanical Engineers Part E Journal of Process Mechanical Engineering, vol. 237, no. 3, pp. 896–906, Jul. 2022, doi: 10.1177/09544089221111585.

[13] J. Chen, Y. Zhang, Z. Chen, G. Gan, and Y. Su, "Impact of porous host materials on the compromise of thermochemical energy storage performance," Renewable Energy, vol. 245, p. 122784, Mar. 2025, doi: 10.1016/j.renene.2025.122784.

[14] L. Wang, Y. Luo, S. Guo, and G. Yang, "Experimental investigation on the thermochemical energy storage performance of MgCl2-coral aggregate composites," Journal of Energy Storage, vol. 116, pp. 116075–116075, Mar. 2025, doi: 10.1016/j.est.2025.116075.

[15] E. Bérut et al., "Simulation of a zeolite thermochemical heat storage reactor: Impact assessment of isotherm model selection," International Journal of Heat and Mass Transfer, vol. 231, pp. 125796–125796, Jun. 2024, doi: 10.1016/j.ijheatmasstransfer.2024.125796.

[16] B. Kieskamp, A. Mahmoudi, and M. Shahi, "A novel multi-reactor system for thermochemical heat storage through detailed modeling of K2CO3 particles," Journal of Energy Storage, vol. 78, p. 110028, Feb. 2024, doi: 10.1016/j.est.2023.110028

[17] M. S. Buker, B. Mempouo, and S. B. Riffat, "Performance evaluation and techno-economic analysis of a novel building integrated PV/T roof collector: An experimental validation," Energy and Buildings, vol. 76, pp. 164–175, Jun. 2014, doi: 10.1016/j.enbuild.2014.02.078.